Applied Clay Science 135 (2017) 485–492

Contents lists available at ScienceDirect

Applied Clay Science

journal homepage: www.elsevier.com/locate/clay

Research paper

Cytotoxicity of natural allophane nanoparticles on human lung cancer A549 cells

Yusuke Toyota [a], Yoko Matsuura [a], Masashi Ito [a], Ryota Domura [a], Masami Okamoto [a,*], Shuichi Arakawa [a], Minoru Hirano [b], Katsunori Kohda [b]

[a] Advanced Polymeric Nanostructured Materials Engineering, Graduate School of Engineering, Toyota Technological Institute, 2-12-1 Hisakata, Tempaku, Nagoya 468 8511, Japan
[b] Toyota Central R&D Labs., Inc., 41-1 Yokomichi, Nagakute, Aichi, 480 1192, Japan

ARTICLE INFO

Article history:
Received 6 September 2016
Received in revised form 21 October 2016
Accepted 21 October 2016
Available online 26 October 2016

Keywords:
Allophane nanoparticles
Cytotoxicity
A549 cells
Quartz crystal microbalance
Cell adhesion

ABSTRACT

Clay minerals are mainly used around traditional cosmetics and industrial products, but currently their target application is continuously expanding into pharmaceutical industry and tissue engineering. To broaden the knowledge of in vitro cytotoxicity of allophane nanoparticles against human cancer cells, the cytotoxicity of both natural and synthetic allophane nanoparticles for cultured human alveolar basal epithelial (A549) cells was examined. For both natural and synthetic allophones, the A549 cell viability was maintained at >70% for concentration up to 3160 μg/mL, implying higher biocompatibility of allophane nanoparticles as compared with that of hectorite nanoparticles. The cell adhesion kinetics coupled with cytotoxic characteristics against A549 cells was analyzed using quartz crystal microbalance (QCM) technique to distinguish the dynamic cell adhesion signatures.

1. Introduction

Clays are commonly used in excipients and/or active substances in the pharmaceutics. Several studies are related with the reduction in the oral absorption of numerous medicines by way of the coadministration with clays. Nevertheless, such interactions may also be used to reach technological and biopharmaceutical advantages. In this regard, naturally abundant clay minerals (e.g., montmorillonite (Mt)) possessing multilayered structure and encapsulated organic compounds could be applied as a drug carrier for pharmaceutical materials (Aguzzi et al., 2007). This was the origin in the use of clays in systems of modern drug release.

During the past five years, the cell-based regenerative researches using clay nanoparticles provided new insights for the tissue engineering/regenerative medicine (TERM) (Kommireddy et al., 2005; Lewkowitz-Shpuntoffa et al., 2009; Dawson et al., 2011; Gaharwar et al., 2011; Mieszawska et al., 2011; Dawson et al., 2012). To enhance cell growth clay particles have been employed as encapsulating components within a polymer matrix. One of these studies demonstrated that the effectiveness of Laponite as an encapsulation medium to store human bone marrow stromal cells (HBMSCs) for 4 weeks. This approach has been applied for stabilization of the tubule formation of cultured human umbilical vein endothelial cells (HUVECs) (Dawson et al., 2011, 2012). In another study, multilayer halloysite shows the better adhesion of human fibroblasts, with fibroblasts maintaining their cellular phenotype (Kommireddy et al., 2005). All those properties of clays have suggested new opportunities to enhance differentiation/proliferation of fibroblast cells for bone regeneration, as well as functions for promoting osteogenesis.

On the other hand, there are only a few reports on toxicological effects upon exposure. High doses of organically-modified Mt with a polymer matrix (ethylene vinyl acetate copolymer) significantly reduced MC3T3-E1 mouse calvaria pre-osteoblasts proliferation (Lewkowitz-Shpuntoffa et al., 2009). Based on past research regarding potential toxicity of Mt particles (Li et al., 2010; Gaharwar et al., 2011; Lordan et al., 2011; Baek et al., 2012; Verma et al., 2012), Mt could cause no acute oral cytotoxic effects at high concentration in mice (up to 1000 mg/kg body weight) after long-time exposure. The Mt particles could be absorbed into the body within 2 h, it was not observed significantly accumulation in any specific organ (Baek et al., 2012). Laponite particles added directly to cell culture media did not exhibit loss of viability of MC3T3-E1 cells at high doses of 35 mg/mL (Gaharwar et al., 2011). Li et al. reported an interesting approach to evaluate the cytotoxicity of exfoliated Mt particles in Chinese hamster ovary (CHO) cells in vitro after 24 h incubation at concentrations up to 1000 μg/mL by using Mt (3-(4,5-dimethylthiazol-2-yl)- 2,5-diphenyl tetrazolium bromide) and LDH (lactate dehydrogenase activity) assays (Li et al., 2010). A low cytotoxicity <1 mg/mL (half maximal inhibitory concentration (IC_{50}) > 1 mg/mL) on CHO cells and dose-dependent effect were found after 24 h incubation. At the same time, the safety of the Mt particles for potential uses in biomedical areas was demonstrated. The researchers observed that

* Corresponding author.
E-mail address: okamoto@toyota-ti.ac.jp (M. Okamoto).

http://dx.doi.org/10.1016/j.clay.2016.10.037
0169-1317/

the Mt particles could accumulate and adhered on the surface of cells. Nevertheless, the cell morphology does not show any obvious changes. Ironically, the presence of clay alters cells in permeability as revealed by releasing LDH. The possible reason behind the mechanism of interacting with living cells is not well explored in the literature. Furthermore, many studies have observed cytotoxicity only at high dose condition. Further information on the potential toxicity of clays and their mechanisms of toxicity are needed to fully understand their hazards.

Allophane (1-2 $SiO_2Al_2O_3$ 5-6H_2O) is a short-range-order clay mineral and occurs in some soils derived from volcanic ejecta and is able to protect the extracellular DNA and RNA molecules from ultraviolet light. The primary particle of the allophane is a hollow spherule with an outer diameter of 3.5–5.0 nm and a wall of about 0.6–1.0 nm thick, which has perforations (Brigatti et al., 2006; Iyoda et al., 2012). The surface area of allophane is as high as ~1000 m^2/g, which is often larger than activated carbon. In addition to this large surface area, the (OH)$Al(OH_2)$ groups exposed on the wall perforations are the source of the pH-dependent charge characteristics of allophane nanoparticles.

Previous study recorded the morphological investigation to provide insight into the adsorption structure and characteristics of single-stranded DNA (ss-DNA) adsorbed by the allophane particles, which was the first time of the real images obtained from microscopic experiment (Matsuura et al., 2013). The adsorption of DNA to mineral surfaces is of great interest because of gene transfer, drug release, bio-adhesion (cell capture) and origins of life studies (Ferris et al., 1996; Joyce, 2002; Trevors and Pollack, 2005).

For some of aforementioned above, advances of clay utilization in bio-related fields prompt us to conduct a toxicology study for clays and clay minerals, at the same time more research seems necessary to establish the sources of potential cytotoxicity of allophane nanoparticles.

In this study, the cytotoxic activity of a natural and synthetic allophane nanoparticles was examined for cultured human alveolar basal epithelial (A549) cells. To better understand the potential toxicity of allophane, quartz crystal microbalance (QCM) is a very powerful tool on the basis of the change in cell morphology during cell adhesion (Marx et al., 2003; Zhu et al., 2012; Kandel et al., 2014; Nowacki et al., 2015). It motivated us to investigate the time development of the dynamic cell adhesion signatures and the effect of clays on the cell adhesion as revealed by the cell viscoelastic index (*CVI*), which reflects the formation of cytoskeleton structure and dynamic viscoelastic features of living cells. The effects of allophane nanoparticles were also compared to those of other clay nanoparticles (hectorite) frequently studied for biological and medical application. Knowledge of such a comparison should also be useful in assessing how does the clay nanoparticles affect the dynamic cell adhesion signatures.

2. Materials and methods

2.1. Allophanes and hectorite

The natural allophane sample was provided by Shinagawa Chemicals Ltd. and designated as AK70. AK70 was treated by H_2O_2 to remove of the humic substance and not further purified for use (Iyoda et al., 2012). The overall size of a single allophane particle is ~5 nm with a specific surface area of 250 m^2/g, which was estimated by the *t*-method (Fig. 1) (Lippens and de Boer, 1965; Iyoda et al., 2012). The functional groups (HO)$Al(OH_2)$ exposed on the wall perforations (defects) play a significant role as active sites in the adsorption process. The Si/Al ratio (=0.58) of the sample was determined by dissolution in acidic ammonium oxalate solution (Theng et al., 1982; Iyoda et al., 2012).

The precursor gels (Si/Al ratio = 0.50, 0.75 and 1.0) for the allophane synthesis were prepared by mixing and stirring (for 1 h) of 100 mM of sodium silicate, ortho ($NaSiO_4$, Nacalai-Tesque) and aluminum chloride hexahydrate ($AlCl_3.6H_2O$, Sigma-Aldrich). The sodium chloride formed was removed by centrifugation at a speed of 5000 rpm for 5 min. The precursors were then autoclaved at 100 °C for 48 h. The synthesized

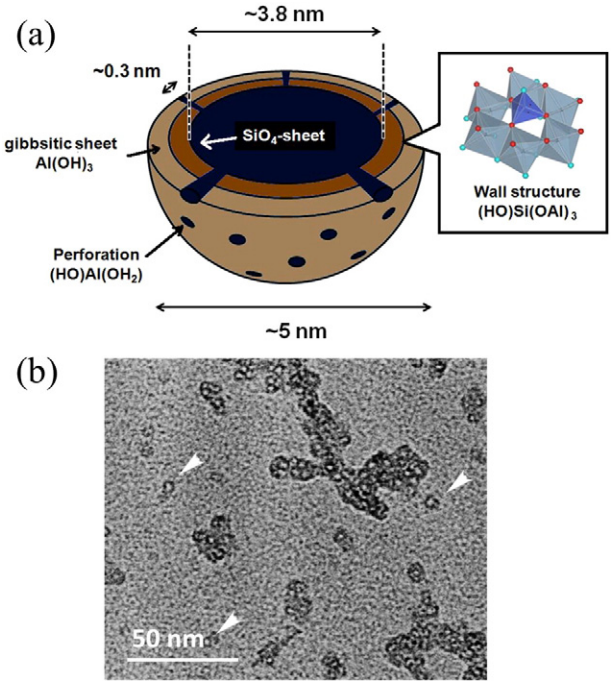

Fig. 1. Allophane structure and TEM bright field image. (a) Schematic representation of allophane structure. The overall size of a single allophane particle is ~5 nm. (b) High resolution TEM image of clustered particles of AK70, rather than singular particles. Arrows indicate single unit particles of allophane [12]. The surface area of allophane is as high as ~1000 m^2/g, which is often larger than activated carbon. (Adapted with permission from [12] Copyright 2012: Elsevier).

samples were designated as allophane(Si/Al)-x (x: Si/Al ratio) and The details of the synthesis experiments were described in previous paper (Iyoda et al., 2012).

Synthetic hydrophilic hectorite clay (SWN) ($Na_{0.33}(Mg_{2.67}Li_{0.33})SiO_4O_{10}(OH)_2$) (thickness ~ 1 nm, diameter ~ 100 nm, and cation exchange capacity = 0.87 meq/g, density = 2.13 g/cm^3) was purchased from CO-OP Chemical Co. Ltd., Japan.

Prior to culture initiation, AK70 nanoparticles were autoclaved and/or sterilized with ethanol at room temperature to assess appropriate sterilization methods.

2.2. Characterization

The surface charge characteristics of both allophane nanoparticles and SWN in water (0.05 wt.%) were determined by electrophoresis (Zetasizer Nano ZS, Malvern Instruments, UK) by the technique of laser Doppler anemometry. The method involved washing AK70 several times with water and adjusting the pH of the dispersion in the range of 2–11 using dilute HCl and NaOH (Nacalai-Tesque). All measurements were performed for four replicates and averaged to get the final value (Kawachi et al., 2013).

The average diameter of the nanoparticles was measured by dynamic light scattering (DLS) using Zetasizer Nano ZS (wavelength = 532 nm). The dynamic information can be retrieved by examining the autocorrelation function $g(t)$ of the time-dependent intensity (Nishida et al., 2015).

2.3. In vitro cell culture and cell viability

Human lung carcinoma A549 cells (ATCC) were used as a cancer cell and were cultured in RPMI-1640 (Wako Pure Chemical Industries) supplemented with 10% FBS including 1% antibiotic-antimycotic mixture. Upon reaching confluence, cells were cultured on 10 cm dishes in an atmosphere of 5% CO_2 and 95% relative humidity at 37 °C.

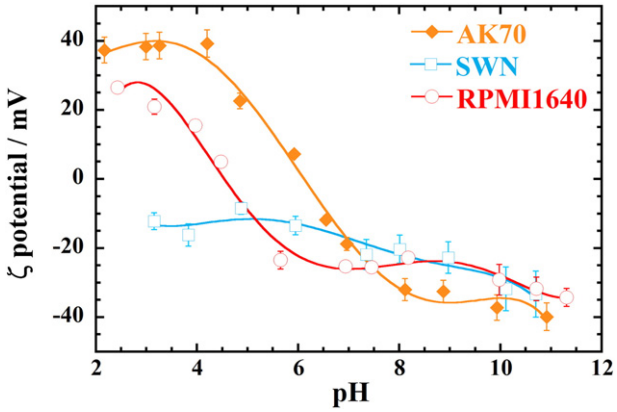

Fig. 2. Zeta potential versus pH of AK70, SWN and RPMI1640 with 10% FBS. Results are expressed as mean ± S.D. (standard deviation) (n = 5).

The cells were seeded in 96-well plates at a cell concentration of 2.0×10^4 cells/cm^2 in 100 μL of medium and cultured for 24 h. Both allophane and SWN dispersions at different concentrations (ranged from 1 to 10,000 μg/mL) were diluted with complete culture medium and added to each well. After incubation for 24 h in an atmosphere of 5% CO_2 and 95% relative humidity at 37 °C, the cell viability was assessed by WST-8 assay (Dojindo) according to manufacturer's instructions. The WST-8 colorimetric test is measuring the activity of intracellular dehydrogenase activity, which is proportional to living cells. The optical density was read on a Multiskan FC (Thermo Fisher Scientific) at 450 nm for the absorbance and at 650 nm for the subtract background absorbance, respectively.

The half maximal inhibitory concentration (IC_{50}) values at 24 h were estimated from the dose-response curves.

2.4. QCM experiment

The QCM (QCM922A, SEIKO EG&G) technique is the simultaneous measurement for the change in resonant frequency (Δf) as mass change and the change in motional resonance resistance (ΔR) as the change of cellular viscoelasticity. AT-cut quartz crystal of fundamental resonant frequency (f_0) of 8.90 MHz with gold electrode (5 mm diameter) was used. The gold surface was washed successively with ethanol and exposed to UV for 10 min. A549 cells in the medium at 1.2×10^5 cells/mL were used in this experiment. 150 μL of the medium containing cells were seeded on the surface of Au electrode attached to Dip-cell mold. The time variation of both f and R values were measured every 1 min up to 12 h for in the incubator maintained in an atmosphere 5% CO_2 and 95% relative humidity at 37 °C. After 90 min incubation, the clay-medium dispersion was administered toward cells monitored by QCM. The cells were allowed to contact and adhere on the gold surface of the sensor. The resonator surface was monitored by the change in f and R.

2.5. Cell morphology

To observe morphology of adherent cells, the attached cells on a 96-well plate were fixed with 3.7% paraformaldehyde (PFA) solution for 20 min. After PFA was removed, cells were washed twice with phosphate buffered saline (PBS), permeabilised with 0.1% Triton X-100, and stained using a 1:40 dilution of DiO (green fluorescence) dye (Sigma) to 2% bovine serum albumin (BSA) in PBS for 20 min in the dark to visualize the cellular morphology and 10 μg/mL solution of Hoechst33342 (Life Technology) in PBS to visualize the nuclei. For visualization of focal contacts vinculin antibody conjugated with Alexafluor 555 (Bioss) diluted in 1% PBS/BSA (1/200 v/v) was added to each well after incubation with allophane and/or SWN with different concentrations, and incubated for 1 h at 37 °C. Between each incubation step, the cells were washed three times with PBS. Cell images were taken on a fluorescent microscope (EVOS® FL Auto, Life Technology).

2.6. Statistics

Statistical analysis was performed using one-way analysis of variance with Williams' post-hoc testing, and significance was considered at a probability of $p < 0.05$.

3. Results and discussion

3.1. Characterization of nanoparticles

The surface charge characteristics of Mt and hectorite possess a negative charge. The surface charge density is particularly important because it determines the interlayer structure of intercalants as well as cation exchange capacity (CEC). Lagaly proposed the method consisting of total elemental analysis and the dimension of the unit lattice cell (Lagaly, 1994):

$$\text{Surface charge} : e^-/nm^2 = \xi/ab \quad (1)$$

where ξ is the layer charge (0.33 for SWN. a and b are cell parameters of SWN ($a = 5.18$ Å, $b = 9.00$ Å (Okamoto et al., 2000)). The zeta potential values for the surface of the SWN are negative over the entire pH range from 3 to 11 and even smaller negative (~ −30 mV) at a higher pH value (Fig. 2).

The surface charge characteristics of allophane are very different from that of SWN. Allophane has a variable of pH-dependent surface charge, because the (HO)Al(OH_2) groups, exposed at surface defect sites, can either acquire or lose protons depending on the pH of the ambient solution. They become $^+$(OH_2)Al(OH_2) by acquiring protons on the acidic side of the point of zero charge (PZC), and become (OH)Al(OH)$^-$ by losing protons on the alkaline side (Fig. 2) (Yuan and Wada, 2012; Kawachi et al., 2013). The PZC of natural allophane, AK70 was (pH) 6.0 in the pH range of 5–7, both positively and negatively charged species are present on the surface of allophane particle. They are able to adsorb cations and anions at the same time (Yuan and Wada, 2012; Kawachi et al., 2013). The synthetic allophane nanoparticles exhibited similar feature in the relationship of zeta potential and pH value (Arakawa et al., 2014).

The culture medium RPMI with 10% FBS shows very similar curve where the PZC shifts to lower pH values (pH 4.7) as compared to AK70. For AK70, the adsorption of ions and proteins from the serum (FBS and BSA) in the cell culture medium. Another interesting point is the comparison with cell membranes at physiological pH values. Due

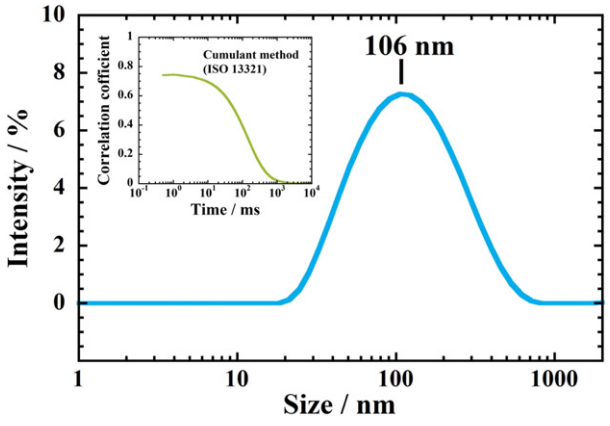

Fig. 3. Particle size distribution of SWN nanoparticles in water (0.05 wt.%) at pH 7.4. The inset is a normalized correlation function (time variation of the correlation coefficient).

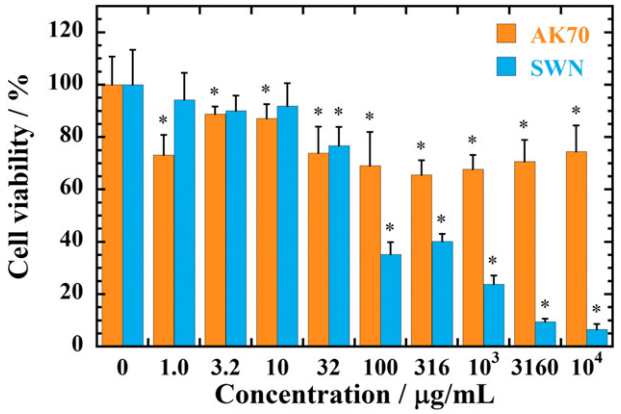

Fig. 4. Cell viability as measured by WST-8 assay using A549 cell after 24 h of incubation with AK70 and SWN of different concentrations. Data were expressed as mean ± S.D. (n = 5). Note: * indicates $p < 0.05$ compared with control.

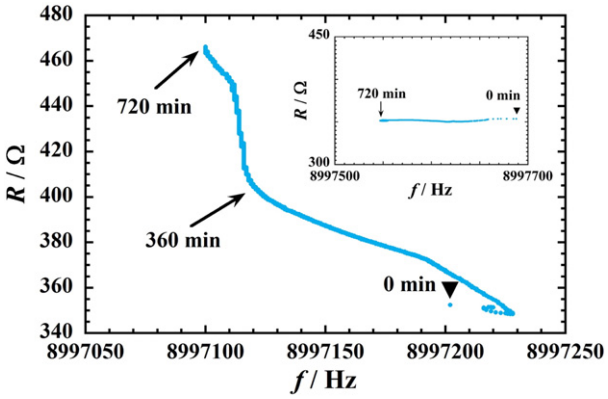

Fig. 6. *R-f* plot of A549 cell adhesion on Au electrode monitored by QCM for 720 min. Arrowheads on the curves indicate on-set time of the cells administration toward medium in Dip-cell mold (0 min). The inset is a *R-f* plot of RPMI-1640 medium monitored by QCM for 720 min.

to the presence of phosphatidylcholine liposomes the total negative charge is provided (~−20 mV) (Bondar et al., 2012). In addition, the cytotoxicity depends on the charge on the surface of the particles. Negatively charged particles at pH 7.40 show lower unfavorable effect on the cells viability because of the negatively charged cell membrane (~−20 mV), which plays an important role to separate the cytoplasm from the outside environment and modulate the movement of the particles in and out of the cell (Xiao et al., 2011; Bondar et al., 2012).

Regarding the aggregation, it is possible to prevent the aggregates formation at high value of zeta potential (~−30 mV) (Doostmohammadi et al., 2011). The aggregation might refer to a necessary charge of repulsive effect between cells and clay particles.

At pH 7.40, the average particle size of SWN is around 100 nm with polydispersity index of 0.36 as revealed by DLS study (Fig. 3). The DLS data also shows that the distribution is clearly asymmetric. Generally, the hydrodynamic radius measured by DLS was much larger than what transmission electron microscopy (TEM) image. The direct interaction between allophane nanoparticles was examined by using TEM at pH 7.0 (Matsuura et al., 2013). The clustered allophane nanoparticle with a width of ~20 nm was observed, indicating the particles are not stabilized electrostatically due to the weak ionic characteristics showing at pH 7.4 (Zeta Potential of Colloids in Water and Waste Water, 1985). All the samples reach an accord with the size (<250 nm), which was the most suitable array in blood circulation.

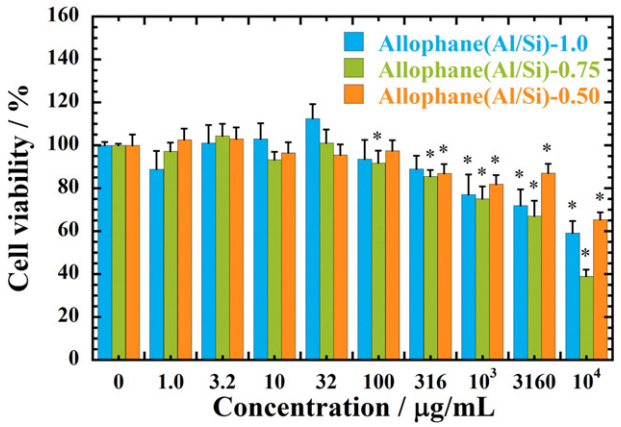

Fig. 5. Cell viability as measured by WST-8 assay using A549 cell after 24 h of incubation with synthetic allophones with three different Si/Al ratios. Data were expressed as mean ± S.D. (n = 5). Note: * indicates $p < 0.05$ compared with control.

3.2. Cytotoxicity of allophane nanoparticles

The effect of the sterilization methods on the cytotoxicity was measured against A549 cells. The cell viability was preserved (ca. 50% of cells survived) up to AK70 concentration of 3160 μg/mL and the characteristics in the cell viability were same without statistically significant difference, regardless of the sterilization methods (i.e., autoclaved, treated with ethanol and untreated) (data not shown). For this reason, the allophane nanoparticles sterilized with ethanol at room temperature was performed in all experiments.

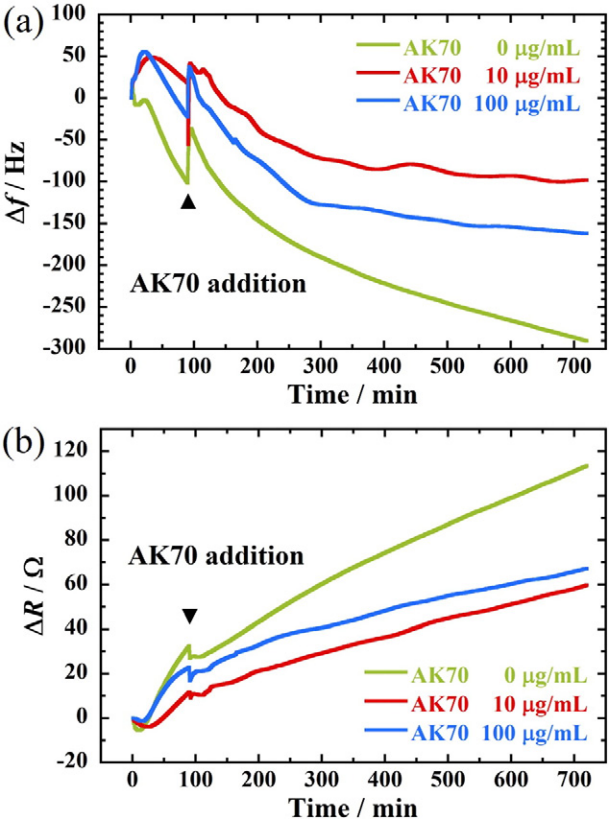

Fig. 7. Real-time variations of (a) Δ*f* and (b) Δ*R* responses for A549 and A549 cells treated with AK70 medium dispersions (10 and 100 μg/mL). Arrowheads on the curves indicate on-set time of the clay administration toward cells (90 min).

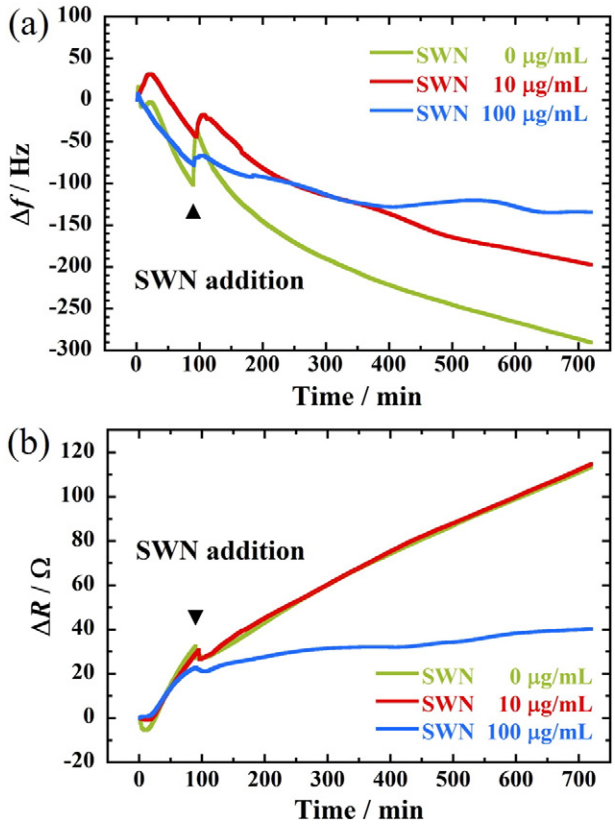

Fig. 8. Real-time variations of (a) Δf and (b) ΔR responses for A549 and A549 cells treated with SWN medium dispersions (10 and 100 μg/mL). Arrowheads on the curves indicate on-set time of the clay administration toward cells (90 min).

As seen in Fig. 4, the AK70 nanoparticles exhibit loss of viability in a concentration- dependency in A549 cells. The cell viability is ca. 70% up to AK70 concentration of 100 μg/mL. With increasing concentration up to 3160 μg/mL, a significant vitality reduction is not observed. WST-8 test demonstrates that the AK70 nanoparticles slightly enhance cell proliferation and viability in the range of 65–85% in comparison with the control. The results demonstrate higher biocompatibility of AK70 without a significant vitality reduction for A549 cells.

For A549 cells incubation with synthetic allophones with three different Si/Al ratios (Fig. 5), their viability is maintained at >70% for concentration up to 3160 μg/mL, implying high biocompatibility of synthetic allophane nanoparticles in a similar characteristic with AK70 nanoparticles. For both AK70 and synthetic allophane nanoparticles, the IC_{50} values for A549 cells are >10,000 μg/mL, suggesting the presence of humic substances and the metallic impurities on the surface of naturally-occurring allophane (AK70) induces very low cytotoxicity (Iyoda et al., 2012).

3.3. Cytotoxicity of SWN nanoparticles

The cytotoxicity of SWN nanoparticles in A549 cells is shown in Fig. 4 as reference clay nanoparticles with different features. The SWN nanoparticles have a high toxicity (damage) beyond concentration of 316 μg/mL for 40% cell viability in the period of 24 h. This feature in cell viability differs from those cultured in presence of AK70. The estimated IC_{50} value is 105 μg/mL that are at least two orders of magnitude higher in toxicity given on A549 cells after 24 h of incubation with allophane(Si/Al)-0.75. The results show the addition of even as much as 10,000 μg/mL of AK70 in cell culture did not kill the tested A549 cells. The AK70 nanoparticles exposure to biological tissue is expected when one applies allophane nanoparticle as a nanocarrier for anti-cancer drug delivery (Ma et al., 2014).

3.4. Dynamic cell adhesion signatures

The typical responses of f and R is shown in the whole cell adhesion processes of A549 cells alone incubated in medium, as the cells sediment toward, contact, and adhere on the gold surface (Fig. 6). The baseline of f- and R-values prior to addition of cells was first evaluated. The inset of Fig. 6 illustrates the R-f plot for medium with 10% FBS for 720 min. The decrease in f is observed, while the R-value remains essentially unchanged as elastic mass binding (Zhu et al., 2012). Following cell addition (marked with the arrowhead at 0 min), the decrease in f and the increase in R are observed due to the dynamic cell adhesion from 20 to 360 min, accompanied with change in R ranged from 350 to 390 Ω. Subsequently, the R-value rapidly increases in the range from 400 to 470 Ω, which is correlated to the spreading of the cells on the gold surface (Zhu et al., 2012).

The typical responses of Δf and ΔR is shown in the whole cell adhesion processes of A549 cells and A549 cells incubated in AK70 medium dispersion, spreading on the electrode (Fig. 7). The adhesion of A549 cells incubated in AK70 medium dispersion progresses slowly, accompanied with little drop in Δf and small increment in ΔR as compared with that of A549 cells alone. For incubation with AK70 dispersion, the decrease in Δf correlates with a decrease in the number of adhered cells. A plateau is reached after incubation for ~700 min. The shift in R reflects changes in the overall cell rigidity that is correlated to the spreading of the cells (Marx et al., 2003). The decrease in ΔR indicates a loss in viscoelasticity within the QCM signal penetration depth (~400 nm). Although there is no clear dose dependency, these Δf and ΔR changes reflect the cell rounding, weak cell surface interactions, and loss of adhesion during cell adhesion processes.

The significant decrease in ΔR and small shift in Δf even for SWN concentration of 100 μg/mL can be interpreted as a decrease in the

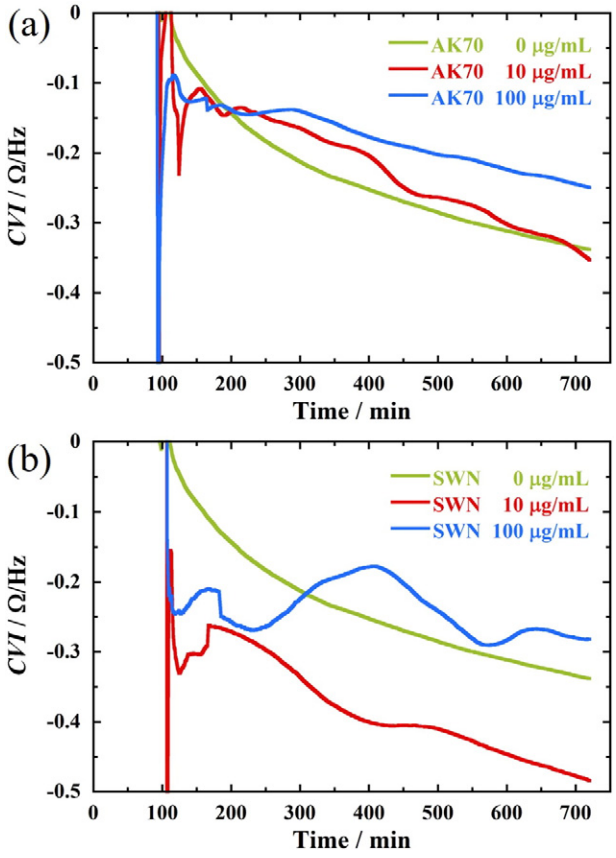

Fig. 9. Time variation of *CVI* for A549 and A549 cells treated with (a) AK70 and (b) SWN medium dispersions at two different concentrations (10 and 100 μg/mL). The on-set time of the clay administration toward cells is 90 min.

Table 1
Parameters of nonlinear regression analyses for A549 cell expansion and adhesion in the presence of clay nanoparticles with different concentrations.

Samples	Responses	$t_{1/2}$/min	p	R^{2a}
A549 (control)	Δf	236	2.20	0.981
	ΔR	369	2.92	0.986
AK70 10 μg/mL	Δf	193	3.08	0.967
	ΔR	369	2.69	0.982
AK70 100 μg/mL	Δf	178	2.87	0.992
	ΔR	321	2.32	0.981
SWN 10 μg/mL	Δf	271	2.51	0.975
	ΔR	369	2.83	0.985
SWN 100 μg/mL	Δf	250	2.70	0.936
	ΔR	266	2.14	0.914

[a] The values are obtained using Eq. (2).

strength of the cell adhesion due to the cells exposed to the IC_{50} value (= 105 μg/mL) (Fig. 8).

The cell number attached to the crystal surface could not be evaluated using large Δf and ΔR differences. For better understanding the useful information based on cell viscosity index ($CVI = \Delta R/\Delta f$) is employed. The *CVI* has no relation to the cell number or the relative positions of the cells on the sensing crystal. The motional resistance *R* reflects both cell surface binding and the involvement of cytoskeletal structures. The large negative value in *CVI* reflects less elastic or the well-organized cytoskeletal structure of the cells (Zhu et al., 2012). The *CVI* value decreases with time in A549 cells, implying the less elastic interior structure as cells spread and flatten on the sensor (Fig. 9).

The incubation with AK 70 indicates that the cell structure in the whole cell adhesion process becomes rather highly interior structure possessing less energy dissipation (small increment in ΔR) with time (as seen in Fig. 7(b)) possibly occurring due to the weak cell surface interactions caused by less cytoskeletal structures (Fig. 9(a)).

In contrast, it is important to note that the A549 incubation with SWN (100 μg/mL) dispersion produces significant different cell adhesion properties on the sensor with the increasing toxicity as compared to that with AK70. The *CVI* value fluctuates and remains almost constant with higher value of ~− 0.27 Ω/Hz (Fig. 9(b)). This speculates the more cell rounding and the weak cell adhesion during the death process. Cell adhesion is thus different from two kinds of clay nanoparticles due to the significant difference in cytotoxicity for A549 cells.

In addition, the QCM dynamic response profile (shape) reflects the cell-cell interactions (Marx et al., 2003). For both Δf and ΔR data in

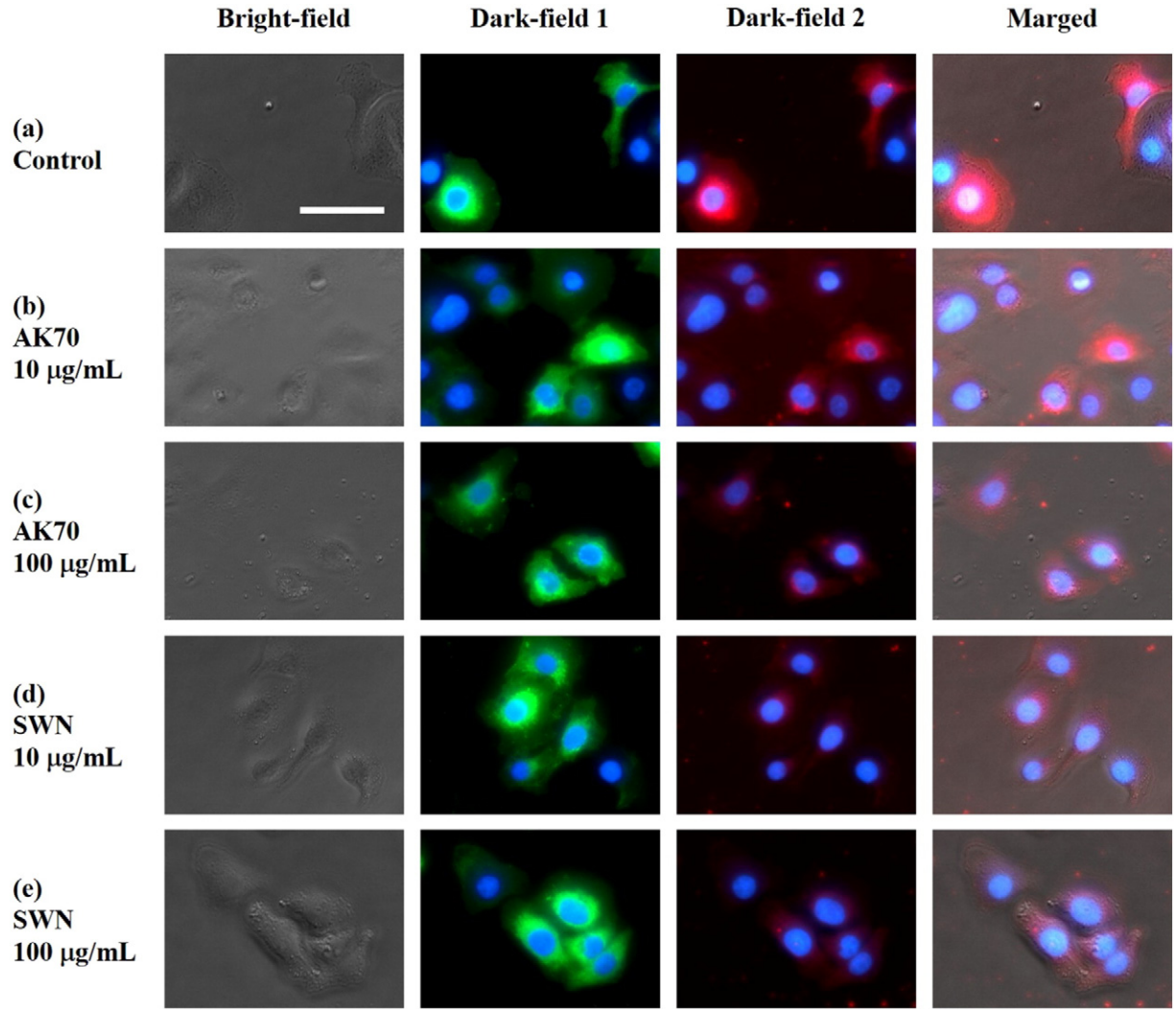

Fig. 10. Representative micrographs of A549 cells incubated for 24 h: (a) without clay nanoparticles, (b) with AK70 medium dispersions for 10 μg/mL, (c) for 100 μg/mL, (d) SWN medium dispersions for 10 μg/mL and (e) for 100 μg/mL. For each panel, images from left to right show bright-field images, dark-field 1 (the cell membrane (green) and the nuclei (blue)), dark-field 2 (the focal contacts with vinculine (red) and the nuclei (blue)), and merged images. The merged images consist of bright-field and dark-field 2 images. Bar represents 50 μm.

the period from 90 to 720 min, the nonlinear regression analysis was performed with Hill equation.

$$Y = A_2 + (A_1 - A_2)/\left[1 + (t/t_{1/2})^p\right] \quad (2)$$

In Eq. (2), QCM response (Y = Δf or ΔR) varies from initial shift A_1 to maximum change A_2, and $t_{1/2}$ is the time at which QCM response is halfway between A_1 and A_2. The ***p*** value is the Hill slope, corresponding to the steepness of the time variation of Δf and ΔR curves. The effects of AK70 medium dispersion (10 and 100 μg/mL) during the cell adhesion are summarized in Table 1. The result obtained from A549 cells incubated in SWN medium dispersion is compared.

For A549 cells, the ***p*** value with ΔR response (2.92) exhibits larger than that with Δf response (2.20), suggesting the involvement of cytoskeletal structures, such as spreading and flattening on the electrode. On the other hand, the opposite feature (***p*** in $\Delta R <$ ***p*** in Δf) is seen in AK70 medium dispersions, where lead to less cell-cell contact accompanied with the loss of adhesion (small shift in Δf as seen in Fig. 7(a)) due to the suppression of the subsequent neighbor cell adhesion. The same feature is observed in the A549 incubation with SWN in the concentration of 100 μg/mL.

3.5. Cell morphology and focal contacts

The cell membrane is observed as green fluorescence and the cell nuclei are stained with Hoechst33342 (blue). The focal contacts appear red fluorescence. After 90 min incubation, the clay-medium dispersions with different concentrations were administered toward cells and the cells were incubated up to 24 h. As shown in Fig. 10, the cells exhibit overwhelming red fluorescence around the nucleus (perinuclear region) when the A549 cells incubated without nanoparticles for 24 h, demonstrating that the cells are able to spread in the adhesion to the substrate (well plate) (Fig. 10(a)), even though the spreading and focal adhesions proceed on the hydrophilic condition as compared to surface hydrophobicity of gold QCM electrode. However, the cells incubated with AK70 nanoparticles (10.0 and 100 μg/mL) produce less spreading with partially staining with vinculin antibody conjugated with Alexafluor 555. The majority of cells present structured polygonal and rounded shape (Fig. 10(b) and (c)). The cell expansion and adhesion in the presence of SWN nanoparticles are very restricted with cells rather rounded and showing little evidence of focal contact formation (Fig. 10(d) and (e)). From these images, SWN has been efficiently reduced the focal contacts in the high concentration (100 μg/mL, Fig. 10(e)). Taken together, these fluorescence images support the QCM dynamic responses in the spreading and adhesion of the A549 cells with clay nanoparticle incubation.

4. Conclusions

The present study has examined the cytotoxicity of a natural and synthetic allophane nanoparticles for cultured human alveolar basal epithelial (A549) cells. The higher cytocompatibility of natural allophane (AK70) nanoparticles without a significant vitality reduction for A549 cells was demonstrated. The cell viability was maintained at >70% for concentration up to 3160 μg/mL for synthetic allophones with three different Si/Al ratios, implying high biocompatibility of synthetic allophane nanoparticles in a similar characteristic with AK70 nanoparticles. The SWN nanoparticles have demonstrated a high toxicity beyond concentration of 316 μg/mL for 40% cell viability in the period of 24 h. For better understanding of cell spreading and adhesion signatures, the useful information based on *CVI* value was employed using the QCM technique. The cell spreading and adhesion were different from two kinds of clay nanoparticles due to the significant difference in cytotoxicity for A549 cells. The AK70 nanoparticles exposure to biological tissue is expected when one applies allophane nanoparticle as a nanocarrier for anti-cancer drug delivery. Further efforts are needed to explore long-term toxicity toward practical applications.

Author contributions

The manuscript was written through contributions of all authors. All authors have given approval to the final version of the manuscripts.

Notes

The authors declare no competing financial interest.

Acknowledgments

This work was supported by a grant in TTI as a Special Research Project (2014). The author (S.A.) was supported, in part, by a research grant 2015, Nippon Sheet Glass Foundation for Materials Science and Engineering.

References

Aguzzi, C., Cerezo, P., Viseras, C., Caramella, C., 2007. Use of clays as drug delivery system: possibilities and limitations. Appl. Clay Sci. 36, 22–36.
Arakawa, S., Matsuura, Y., Okamoto, M., 2014. Allophane-Pt nanocomposite: synthesis and MO simulation. Appl. Clay Sci. 95, 191–196.
Baek, M., Lee, J.A., Choi, S.J., 2012. Toxicological effects of a cationic clay, montmorillonite in vitro and in vivo. Mol. Cell. Toxicol. 8, 95–101.
Bondar, O.V., Saifullina, D.V., Shakhmaeva, I.I., Mavlyutova, I.I., Abdullin, T.I., 2012. Monitoring of the zeta potential of human cells upon reduction in their viability and interaction with polymers. Acta Nat. 1 (12), 78–81.
Brigatti, M.F., Galan, E., Theng, B.K.G., 2006. Structures and mineralogy of clay minerals. In: Bergaya, F., Theng, B.K.G., Lagaly, G. (Eds.), Handbook of Clay Science. Elsevier, Amsterdam, pp. 19–86.
Dawson, J.I., Kanczler, J.M., Yang, X.B., Attard, G.S., Oreffo, R.O.C., 2011. Clay gels for the delivery of regenerative microenvironments. Adv. Mater. 23, 3304–3308.
Dawson, J.I., Kingham, E., Evans, N.R., Tayton, E., Oreffo, R.O.C., 2012. Skeletal regeneration: application of nanoto-pography and biomaterials for skeletal stem cell based bone repair. Inflammation Regener. 32, 72–89.
Doostmohammadi, A., Monshi, A., Salehi, R., Fathi, H.F., Golniya, Z., Daniels, U.A., 2011. Bioactive glass nanoparticles with negative zeta potential. Ceram. Int. 37, 2311–2316.
Ferris, J.P., Hill, A.R., Liu, R.H., Orgel, L.E., 1996. Synthesis of long prebiotic oligomers on mineral surfaces. Nature 381, 59–61.
Gaharwar, A.K., Schexnailder, P.J., Kline, B.P., Schmidt, G., 2011. Assessment of using Laponite® cross-linked poly(ethylene oxide) for controlled cell adhesion and mineralization. Acta Biomater. 7, 568–577.
Iyoda, F., Hayashi, S., Arakawa, S., Okamoto, M., 2012. Synthesis and adsorption characteristics of hollow spherical allophane nano-particles. Appl. Clay Sci. 56, 77–83.
Joyce, G.F., 2002. The antiquity of RNA-based evolution. Nature 418, 214–221.
Kandel, J., Lee, H.S., Sobolewski, P., Tomczyk, N., Composto, R.J., Eckmann, D.M., 2014. Chemically grafted fibronectin for use in QCM-D cell studies. Biosens. Bioelectron. 58, 249–257.
Kawachi, T., Matsuura, Y., Iyoda, F., Arakawa, S., Okamoto, M., 2013. Preparation and characterization of DNA/allophane composite hydrogels. Colloids Surf. B 112, 429–434.
Kommireddy, D., Ichinose, I., Lvov, Y., Mills, D., 2005. Nanoparticle multilayer: surface modification for cell attachment and growth. J. Biomed. Nanotechnol. 1, 286–290.
Lagaly, G., 1994. Layer charge determination by alkylammonium ions. In: Mermut, A.R. (Ed.), Layer Charge Characteristics of Clays, CMS Workshop Lectures 6. The Clay Minerals Society, Boulder, Colorado, pp. 1–16.
Lewkowitz-Shpuntoffa, H.M., Wenb, M.C., Singhc, A., Brennerd, N., Gambinod, R., Pernodetd, N., Isseroffe, R., Rafailovichd, M., Sokolovd, J., 2009. The effect of organo clay and adsorbed FeO3 nanoparticles on cells cultured on ethylene vinyl acetate substrates and fibers. Biomaterials 30, 8–18.
Li, P.R., Wei, J.C., Chiu, Y.F., Su, H.L., Peng, F.C., Lin, J.J., 2010. Evaluation on cytotoxicity and genotoxicity of the exfoliated silicate Nanoclay. ACS Appl. Mater. Interfaces 2, 1608–1613.
Lippens, B.C., de Boer, J.H., 1965. Studies on pore systems in catalysts: V. The t method. J. Catal. 4, 319–323.
Lordan, S., Kennedy, J.E., Higginbotham, C.L., 2011. Cytotoxic effects induced by unmodified and organically modified nanoclays in the human hepatic HepG2 cell line. J. Appl. Toxicol. 31, 27–35.
Ma, R., Wang, Z., Yan, L., Chen, X., Zhu, G., 2014. Novel Pt-loaded layered double hydroxide nanoparticles for efficient and cancer-cell specific delivery of a cisplatin prodrug. J. Mater. Chem. B 2, 4868–4875.
Marx, K.A., Zhou, T., Warren, M., Braunhut, S.J., 2003. Quartz crystal microbalance study of endothelial cell number dependent differences in initial adhesion and steady-state behavior: evidence for cell-cell cooperativity in initial adhesion and spreading. Biotechnol. Prog. 9, 987–999.

Matsuura, Y., Iyoda, F., Arakawa, S., John, B., Okamoto, M., Hayashi, H., 2013. DNA adsorption characteristics of hollow spherule allophane nano-particles. Mater. Sci. Eng. C 33, 5079–5083.
Mieszawska, A.J., Llamas, J.G., Vaiana, C.A., Kadakia, M.P., Naik, R.R., Kaplan, D.L., 2011. Clay enriched silk biomaterials for bone formation. Acta Biomater. 7, 3036–3041.
Nishida, Y., Domura, R., Sakai, R., Okamoto, M., Arakawa, S., Ishiki, R., Salick, M.R., Turng, L., 2015. Fabrication of PLLA/HA composite scaffolds modified by DNA. Polymer 56, 73–81.
Nowacki, L., Follet, J., Vayssade, M., Vigneron, P., Rotellini, L., Cambay, F., Egles, C., Rossi, C., 2015. Real-time QCM-D monitoring of cancer cell death early events in a dynamic context. Biosens. Bioelectron. 64, 469–476.
Okamoto, M., Taguchi, H., Sato, H., Kotaka, T., Tateyama, H., 2000. Dispersed structure and rheology of lipophilized-smectite/toluene suspensions. Langmuir 16 (9), 4055–4058.
Theng, B.K.G., Russell, M., Churchman, G.J., Parfitt, R.L., 1982. Surface properties of allophane, halloysite, imogolite. Clay Clay Miner. 30, 143–149.
Trevors, J.T., Pollack, G.H., 2005. Hypothesis: the origin of life in a hydrogel environment. Prog. Biophys. Mol. Biol. 89, 1–8.
Verma, N.K., Moore, E., Blau, W., Volkov, Y., Babu, P.R., 2012. Cytotoxicity evaluation of nanoclays in human epithelial cell line A549 using high content screening and real-time impedance analysis. J. Nanopart. Res. 14, 1137–1147.
Xiao, K., Li, Y., Luo, J., Lee, J.S., Xiao, W., Gonik, A.M., Agarwal, R.G., Lam, K.S., 2011. The effect on surface on in vivo biodistribution of PEG-oligocholic acid based micellar nanoparticles. Biomaterials 32, 3435–3446.
Yuan, G., Wada, S.I., 2012. Allophane and imogolite nanoparticles in soil and their environmental applications. In: Barnard, A.S., Guo, H.B. (Eds.), Nature's Nanostructures. Pan Stanford Publishing Pte. Ltd., Shingapore, pp. 485–508.
Zeta Potential of Colloids in Water and Waste Water, 1985. ASTM Standard D (4187-4182).
Zhu, T., Marx, K.A., Dewilde, A.H., Mclntosh, D., Braunhut, S.J., 2012. Dynamic cell adhesion and viscoelastic signatures distinguish normal from malignant human mammary cells using quartz crystal microbalance. Anal. Biochem. 421, 164–171.